

# Computational investigation of the ionic conductance through molybdenum disulfide (MoS<sub>2</sub>) nanopores

María Daniela BARRIOS PEREZ<sup>1</sup>, Patrick SENET<sup>1,†</sup>, Vincent MEUNIER<sup>2</sup>, Adrien NICOLAI<sup>1,‡</sup>

<sup>1</sup>Laboratoire Interdisciplinaire Carnot de Bourgogne UMR 6303 CNRS-Université de Bourgogne Franche-Comté, 9 Avenue Alain Savary, BP 47870, F-21078 Dijon Cedex, FRANCE.

<sup>2</sup>Department of Physics, Applied Physics, and Astronomy, Rensselaer Polytechnic Institute, 110 8th street, Troy, NY 12180, USA.

Corresponding authors: <sup>†</sup>psenet@u-bourgogne.fr, <sup>‡</sup>adrien.nicolai@u-bourgogne.fr

**Abstract:** Solid-state nanopores have emerged as versatile devices for probing single molecules. Because the channel conductance of the ionic flow through nanopores scales inversely with the membrane thickness, few-atoms thick materials are ideal candidates with an expected high signal-to-noise ratio. On one hand, graphene nanopores have been extensively studied because they exhibit the highest signal. However, they also exhibit high noise. On the other hand, transition metal dichalcogenides such as molybdenum disulfide (MoS<sub>2</sub>) are potentially advantageous due to their rich optoelectronic and mechanical properties. In this paper, we investigate the dynamics of KCl ions through MoS<sub>2</sub> nanopores using non-equilibrium molecular dynamics (MD) simulations. MoS<sub>2</sub> nanopores with different diameters, from 1.0 to 3.0 nm and nanoporous membranes with different thicknesses, from single-layer to trilayers MoS<sub>2</sub> are studied. The structural properties of ions and water inside MoS<sub>2</sub> nanopores are discussed and the performance of MoS<sub>2</sub> nanopores to conduct ions at low voltages is quantified by computing I-V curves in order to extract open pore conductance and by comparing MD data to analytical models. This comparison reveals that ionic conductance and *effective* geometrical parameters for MoS<sub>2</sub> nanoporous membranes extracted from models are overestimated. We provide open pore benchmark signals for further translocation simulations/experiments using MoS<sub>2</sub> nanopores.

**Key-Words:** nanopores, MoS<sub>2</sub>, MD simulations, open pore conductance, bulk conductivity, effective diameter, effective thickness

## 1 Introduction

Solid-state nanopores (SSN), which are typically synthesized using stimuli-responsive materials as the body component, arise as sensor for the detection of single molecules [1]. One of the highest-profile applications of SSN is DNA sequencing, as they hold the potential to do that faster and cheaper than current industrial standards [2]. SSN sequencing is based on experimental measurement of the variations in ionic current as the molecules translocate through nanometer-sized channels when an external voltage is applied across the membrane. As charged molecules in ionic solution pass through nanopores, they displace ions from the pore volume. Therefore, ultrafast monitoring of ion flow [3] during the passage of a particle through SSN yields information about the particle structure and chemical properties. Precisely, SSN detect the presence of individual molecules via a change in ionic conductance  $\Delta G$ .  $\Delta G$  represents a drop in ionic conductance, such as  $\Delta G = G_0 - G_m$ , where  $G_0$  is the open pore conductance and  $G_m$  is the conductance when the

nanopore is obstructed by a translocating molecule, also called translocation conductance. Therefore, increasing  $\Delta G$  and decreasing the signal noise yield a higher signal-to-noise ratio (SNR). Thus, assuming constant noise, increasing  $\Delta G$  improves the performance of nanopore devices. Hence, the magnitude and statistical properties of  $\Delta G$  provide good metrics for the nanopore sensing capability [4].

For instance, if the molecule translocating through a SSN is characterized by the same size as the pore dimension, for instance a double strand DNA molecule translocating in a SSN of diameter  $D \sim 2.2$  nm, the theoretical conductance drop is equal to the open pore conductance,  $\Delta G = G_0$ . In order to fabricate DNA sequencing devices with a high-resolution recognition and detection of DNA bases, the diameter of the nanopore must be of the same order of magnitude as that of the molecule to be detected. SSN are characterized by two parameters: the diameter of the pore  $D$  and the thickness of the membrane  $h$ . These two parameters can be easily characterized in all-atom simulations compared to

experiments where they are usually estimated and named *effective* parameters. Since the diameter of the pore is chosen according to the size of the molecule that is probed, the thickness  $h$  is the controllable parameter. Therefore, nanopores drilled in solid-state thin films improve significantly the signal for molecule detection because the conductance of the ionic flow through SSN scales inversely with the nanoporous membrane thickness [5]. It follows that both the magnitudes of the open pore current  $G_0$  and of the blockade current  $G_m$  increase with the decreasing thickness of the film.

Based on the above discussion, ultra-thin membranes are thus ideal candidates for single-molecule sequencing with a high SNR. Over the past decade, stable nanomaterials have enabled the investigation of advanced thin-film nanopores, in which single-residue discrimination should be possible and has already been done using biological nanopores [8]. For example, graphene nanopores have emerged as ideal candidates due to the fact they exhibit the highest signal (one-atom thick layer). In particular, experiments on DNA translocation through single-layer graphene nanopores have been successfully performed in 2010 by three independent groups [9–11]. However, the high noise that characterizes graphene nanopores experimentally have made them poor devices [12], leading to a SNR around 3.5. Furthermore, efforts to fabricate nanoporous membranes including thinning silicon nitride ( $\text{SiN}_x$ ) films can be an alternative path but drilling a nanometer-sized pore with reactive-ion etching [6, 7] or using an electron beam [4] is very sensitive to the mechanical strength of such thin-films. For instance, in a previous work on amorphous silicon (a-Si) membranes, we showed that the thickness limit lies at about 1.0 nm [4]. In parallel to experiments, molecular dynamics (MD) simulations were also performed to study the performances of solid-state nanopores for DNA translocation through ionic current measurements [13]. In particular, graphene nanopores have been extensively studied [14–16].

New two-dimensional (2-D) materials in which nanopores can be drilled experimentally with a high reproducibility are therefore needed. Transition-metal dichalcogenides (TMD) are a class of 2-D materials in the form of  $\text{MeX}_2$  (Me = transition metal such as Mo, W, Ti, Nb, etc. and X = S, Se, or Te), which are potentially advantageous for SSN applications due to their rich optoelectronic and mechanical properties [17]. Structurally, one layer of Me atoms is sandwiched between two layers of X atoms and TMD bulk crystals are formed of monolayers bound to each other by van der Waals

(vdW) attraction (Figure 1a). In addition, encouraging experimental results on  $\text{MoS}_2$  nanopores published in 2014 indicate improved signal-to-noise ratio ( $\text{SNR} > 10$ ) [18], ease of DNA translocation, and no special surface treatment requirement. However, the diameters of the nanopores studied in this early work were too large for DNA sequencing (from 5 to 20 nm). Since then, only one computational study has been carried out on DNA base detection using a single-layer  $\text{MoS}_2$  [19].

In the present paper, we focus on the open pore conductance of a 1M KCl ionic solution through  $\text{MoS}_2$  nanoporous membranes using classical MD simulations. SSN with diameters ranging from 1.0 to 3.0 nm are studied here. The characteristics of SSN with a diameter  $D = 2.0$  nm made of single-layer (SL), bilayers (BL) and trilayers (TL)  $\text{MoS}_2$  are also presented (Figure 1). Current-voltage characteristics ( $I$ - $V$  curves), water distribution around  $\text{MoS}_2$  nanoporous membranes and concentration of ions inside SSN are discussed. Finally, the data extracted from MD simulations are compared to a theoretical model commonly used to characterize ionic conductance and *effective* parameters of SSN in experiments [5, 6], with a combination of access resistance and pore resistance:

$$\frac{1}{G} = R = R_{\text{access}} + R_{\text{pore}} = \frac{1}{D\sigma} + \frac{4h}{\pi\sigma D^2} \quad (1)$$

where  $D$  is the pore diameter,  $\sigma$  is the ionic bulk conductivity, and  $h$  is the thickness of the membrane. The aim of this work is to provide a benchmark of expected open pore conductances  $G_0$  and to estimate ideal conductance drops  $\Delta G$  of  $\text{MoS}_2$  nanopores for further simulations/experiments. A comparison of  $\text{MoS}_2$  with graphene nanopores is also discussed.

## 2 Materials and Methods

### 2.1 System Setup

Initially,  $\text{MoS}_2$  layers were constructed using 2-D unit cell lattice vectors  $\vec{a} = (3.13, 0, 0)$  and  $\vec{b} = (0, 5.42, 0)$ . Each rectangular unit cell for  $\text{MoS}_2$  has 6 atoms, 2 Mo and 4 S atoms. The Mo-S bond length was taken as  $d_{\text{Mo-S}} = 2.38$  Å and the S-S distance was taken as  $d_{\text{S-S}} = 3.11$  Å. The unit cell was replicated in both  $x$  and  $y$  direction in order to generate layers of dimension  $10 \times 10$  nm<sup>2</sup>. For multiple-layers  $\text{MoS}_2$  membranes, as shown in Figure 1a, the interlayer spacing was taken as  $d_{\text{is}} = 3.15$  Å.  $\text{MoS}_2$  pores were constructed by removing atoms whose coordinates satisfy  $x^2 + y^2 < R^2$ , where  $D = 2R$  is the diameter of the

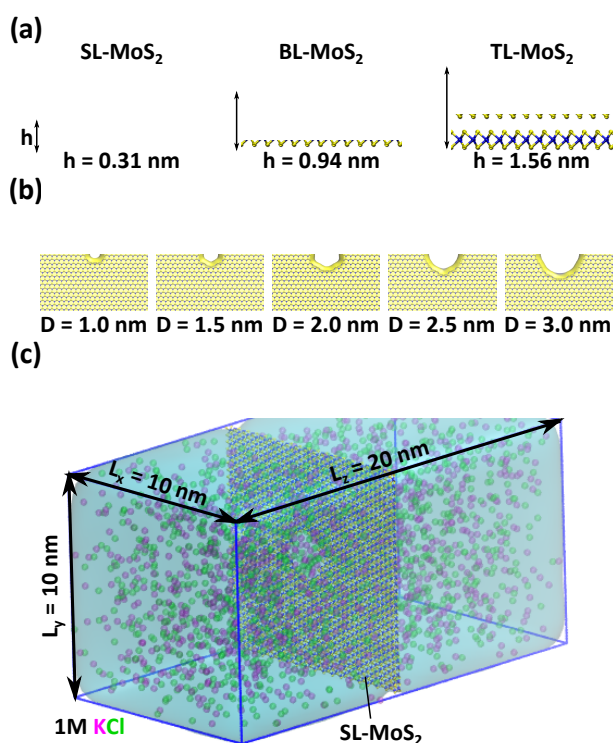


**Figure 1:** (a) All-atom structures of the MoS<sub>2</sub> membranes studied in the present work. MoS<sub>2</sub> membranes are shown in ball and stick representations with Mo atoms colored in blue and S atoms in yellow. Single-layer (SL), bilayers (BL) and trilayers (TL) MoS<sub>2</sub> are shown with their respective thicknesses. (b) All-atom structures of the MoS<sub>2</sub> nanopores studied in the present work. The color code is the same as in panel a. (c) Snapshot of MD simulation of ion transport through a SL-MoS<sub>2</sub> nanopore. Nanopore diameter is  $D = 2.0$  nm. Water molecules are represented by a blue surface. K<sup>+</sup> and Cl<sup>-</sup> ions are represented by magenta and green spheres, respectively.

pore and considering the center of the pore at the origin of the box. The pore diameters that we considered in this work are 1.0, 1.5, 2.0, 2.5 and 3.0 nm, as shown in Figure 1(b). A Stillinger-Weber (SW) potential was used during MD simulations to characterize Mo-S interactions [20].

A MoS<sub>2</sub> nanoporous membrane is located at the center of the simulation box of dimension  $L_x \times L_y \times L_z = 10 \times 10 \times 20$  nm<sup>3</sup>, filled with water molecules and 1M KCl. It represents more than 62,000 water molecules and more than 2,400 ions. The non-bonded interactions between MoS<sub>2</sub> nanopore, water and ions were described using a Lennard-Jones (LJ) plus Coulomb potential. The water model used in the present work is the TIP3P model [21]. LJ parameters for K<sup>+</sup> and Cl<sup>-</sup> ions were taken from reference [22], where specific parameters were developed for the water model employed. LJ parameters for Mo and S atoms were taken from reference [23], as already used in other works [24]. Lorentz-Berthelot mixing rules were applied to

compute cross-interactions between the different species.

For graphene nanopores, the same procedure was followed using the same dimension for the nanoporous membranes. 2-D unit cell lattice vectors are  $\vec{a} = (2.46, 0, 0)$  and  $\vec{b} = (0, 4.26, 0)$ . Each rectangular unit cell for graphene has 4 C atoms. The C-C bond length was taken as  $d_{C-C} = 2.46$  Å. C-C interactions during MD simulations were described using a Tersoff potential [25]. Water model and LJ parameters for ions are the same as for MoS<sub>2</sub>. Finally, LJ parameters for C atoms were taken from reference [26].

## 2.2 Non-equilibrium MD simulations

Non-equilibrium MD simulations (NEMD) were performed using the LAMMPS software package [27] employing periodic boundary conditions in all directions. An external applied electric field was used to investigate ionic currents and conductance through MoS<sub>2</sub> and graphene nanopores. Before running the MD part, an equilibration of the system in the  $NPT$  ensemble ( $T = 300$  K and  $P = 1$  bar) without any electric field was performed during 100 ps to relax the simulation box and the solvent at the target temperature and pressure. Relaxation was followed by MD runs of 10 ns carried out in the  $NVT$  ensemble using the velocity-Verlet algorithm [28] with a time step of 1 fs. A Nosé-Hoover thermostat [29, 30] was used to maintain the temperature at 300 K with a time constant of 0.1 ps. Particle-particle particle-mesh method [31] was used to describe long range electrostatic interactions. A cutoff of 1.0 nm was applied to LJ and Coulomb potential for non-bonded interactions. A SHAKE algorithm [32] was used to constrain the bond lengths and angle of TIP3P water molecules. Finally, simulations were carried out by applying a uniform electric field, directed normal to the nanoporous membrane ( $z$ -direction), to all atomic partial charges in the system. The corresponding applied potential is  $V = EL_z$ , where  $L_z$  is the length of the simulation box in the  $z$ -direction. For each system presented in Table 1, simulations with  $V = 0, 0.25, 0.5, 0.75, 1.0, 1.5, 2.0, 2.5$  and 3.0 V were performed.

## 2.3 Data Analysis

### Ionic current

In order to compute the current-voltage ( $I - V$ ) characteristics of MoS<sub>2</sub> nanopores, we computed the

total net ionic current  $I(t)$  as

$$I(t) = \frac{1}{\Delta t L_z} \sum_{i=1}^N q_i [z_i(t + \Delta t) - z_i(t)] \quad (2)$$

where  $\Delta t$  is the time between MD frames chosen to be 10 ps here),  $L_z$  is the dimension of the simulation box in the  $z$ -direction, which is the direction of the applied electric field,  $N$  is the total number of ions,  $q_i$  is the charge of the ion  $i$  and  $z_i(t)$  is the  $z$ -coordinate of the ion  $i$  at time  $t$ . Ionic currents reported later are computed as the simple moving average of the 10 ns MD runs. The standard error of the ionic current was computed using  $\sigma/\sqrt{N_f}$ , where  $N_f$  is the number of frames used for calculating the average current and  $\sigma$  is the standard deviation. Error bars are of the order of magnitude of 0.2 nS for MoS<sub>2</sub> nanopores of diameter  $D = 2.0$  nm with an applied voltage  $V = 1.0$  V. Therefore, they are not represented in  $I - V$  curves shown in Figure 2.

### Normal and in-plane radial distributions of water

In order to estimate the *effective* thickness and diameter of the different nanoporous membranes made of MoS<sub>2</sub> layers, we computed the radial distribution of water molecules inside the pore ( $\rho$  direction) as well as the distribution of water molecules in the direction normal to the membrane ( $z$  direction here). First, the normal distribution was computed by counting the number of water molecules in boxes of dimension  $L_x \times L_y \times \Delta z$ , with  $\Delta z = 1$  Å. Starting from the membrane, the box was displaced by 0.1 Å in the normal direction up to reaching the top of the simulation box. Second, the in-plane radial distribution of water was computed over concentric cylinders with the pore axis. Each ring is characterized with a height corresponding to the  $z$ -position of the center of the nanopore  $\pm 1$  Å (total height of 2 Å) and with a 1 Å width from the inner to the outer boundaries. Starting from the center of the pore, the inner boundary of each cylinder was displaced by 0.25 Å in the radial direction, up to reaching the nanopore edge. The radial and normal distributions reported below were averaged over the 10 ns MD runs with voltages  $0 < V \leq 1.0$  V, for a total duration of 40 ns (4 runs).

### Radial ionic concentration

In order to investigate the ion distribution inside the nanopores and particularly near the nanopore edges, we computed the ion concentration (number of ions/nm<sup>3</sup>) as a function of the radial distance  $\rho$

from the center of the pore ( $\rho = 0$ ) from MD trajectories. For that purpose, we averaged the ion concentration over concentric cylinders with the pore axis. Each ring has a height corresponding to the *effective* height of the nanopore  $h_{eff}$  and a width of 1 Å from the inner to the outer boundaries. Starting from the center of the pore, the inner boundary of each cylinder was displaced by 0.25 Å in the radial direction, up to reaching the nanopore edge. The radial ionic concentrations reported below are average values over positively and negatively charged ions, for the 10 ns MD runs with voltages  $0 < V \leq 1.0$  V, for a total duration of 40 ns (4 runs).

## 3 Results and Discussion

### 3.1 Current-Voltage characteristics

$I - V$  curves for each system were computed as explained in section 2 and are presented in Figure 2. First,  $I - V$  curves were only computed from simulation with positive voltages since nanoporous membranes made of graphene and MoS<sub>2</sub> are symmetric and extremely thin along the normal direction of the membrane ( $z$ -direction). Therefore, no ionic rectification is observed [33]. However, negative voltages were tested for one system (SL-MoS<sub>2</sub> with  $D = 2.0$  nm) and the absence of rectification was confirmed (data not shown).

From simulations with  $V = 0$  to 3.0 V, two types of regime were detected: a linear regime from 0 to 1.0 V, corresponding to an ohmic behavior of the nanopore, and a sublinear regime from 1.0 to 3.0 V (inset Figure 2a). Several interpretations of the physical meaning of this sublinear behavior of  $I - V$  curves at high voltages are still being debated in the literature. In particular, permeation of ions through small confined spaces such as ionic channels has been considered diffusion-limited. Recently, in contrast with the permeation theory, factors such as ion hydration and their configurational restraint due to the coordination with water molecules while crossing the channel, can induce a free-energy barrier that leads to a saturation of the current  $I$  at high voltages [34]. In the present work, we only focus on the linear part of the  $I - V$  curves since experimentally, the applied voltages are usually of magnitude of several hundreds of mV at maximum. The values of open pore conductance were extracted from the linear response regime, as the slope of the  $I - V$  characteristics.

By comparing graphene and MoS<sub>2</sub> nanopores of diameter  $D = 2.0$  nm, we observed that the slope of the  $I - V$  curves are relatively close, leading to open

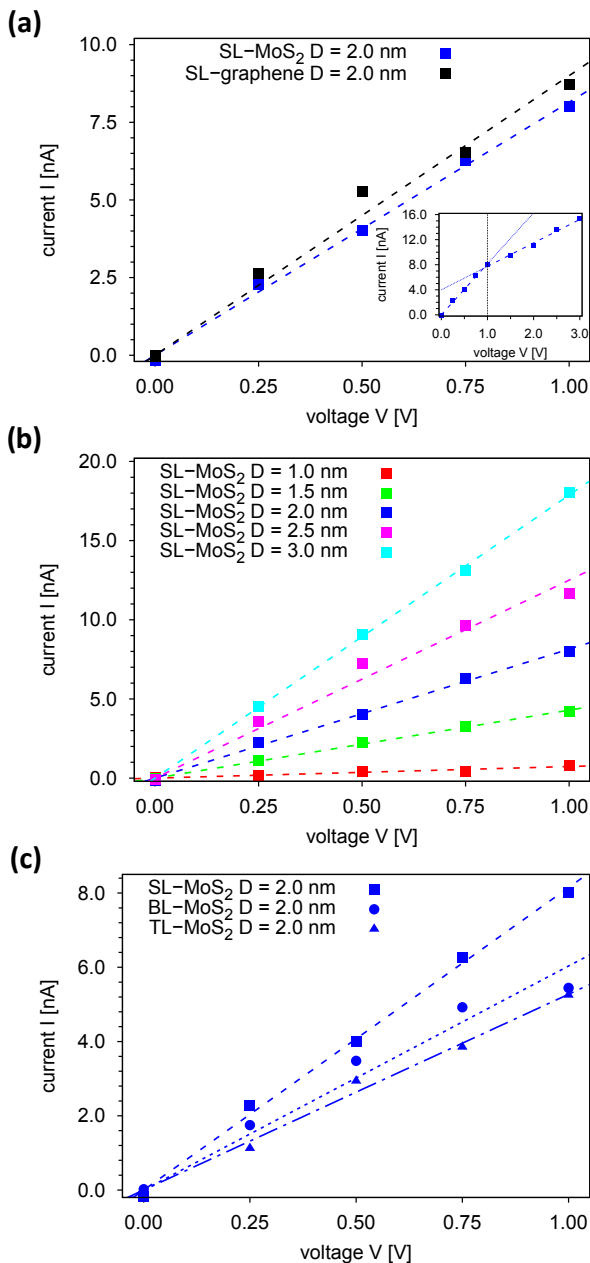


**Figure 2:** Current-voltage  $I - V$  characteristics of nanopores studied in the present work. Data from 0 to 1.0 V are shown except inset of panel a. (a)  $I - V$  curves for single-layer graphene (black) and MoS<sub>2</sub> (blue) nanopores of diameter  $D = 2.0$  nm. The inset in panel a represents the  $I - V$  curve for MoS<sub>2</sub> up to 3.0 V. (b)  $I - V$  curves for single-layer MoS<sub>2</sub> nanopores of diameter  $D = 1.0$  (red), 1.5 (green), 2.0 (blue), 2.5 (magenta) and 3.0 nm (cyan). (c)  $I - V$  curves for single-layer (blue squares), bilayers (blue circles) and trilayers (blue triangles) MoS<sub>2</sub> nanopores of diameter  $D = 2.0$  nm. Dashed lines represent the linear behavior fitted onto the MD data. Open pore conductances  $G_0$  were obtained as the slope of the linear fits.

pore conductances  $G_0$  of 9.0 and 8.1 nS, respectively. Despite the fact that MoS<sub>2</sub> has a thickness larger than graphene, it can still be considered as an ultra-thin membrane. In addition, MD simulations show that a

diameter  $D = 1.0$  nm is a critical diameter for MoS<sub>2</sub> nanopores since  $G_0$  is around 0.7 nS, whereas  $G_0 = 4.3$  nS for  $D = 1.5$  nm (Table 1). Finally, we compared open pore conductances  $G_0$  of SL, BL and TL-MoS<sub>2</sub>. As shown in panel c of Figure 2, there is a difference of 2.1 nS between SL and BL-MoS<sub>2</sub>, which represents a variation of  $\sim 30\%$  by increasing the thickness by a factor 3. However, there is no significant difference between BL and TL-MoS<sub>2</sub> (0.8 nS). It means that TL-MoS<sub>2</sub> could be a efficient alternative to BL-MoS<sub>2</sub> in terms of open pore conductances  $G_0$  and fabrication process since at the nanoscale, manipulating thicker objects is easier. Furthermore, it has been shown for graphene that the noise reduces with layer thickness [12].

### 3.2 Interfacial interactions of water with MoS<sub>2</sub> nanoporous membranes and effective geometrical parameters

Experimentally, in lieu of using techniques to measure the geometrical parameters of the nanoporous membranes (diameter  $D$  and thickness  $h$ ) that might deteriorate the sample, the measured  $G_0$  is used to extract the *effective* pore diameter  $D_{eff}$  and membrane thickness  $h_{eff}$  using a cylindrical model for nanopore conductance [4, 5]. Using MD simulations, *effective* parameters can also be extracted and in particular by characterizing the interfacial interactions between the solvent and the nanoporous membrane. In fact, the interactions at the interface between a SSN and the ionic solution made of water molecules and K<sup>+</sup> and Cl<sup>-</sup> ions are strongly influenced by the nature of the 2-D materials and can be fully described at the atomic level using all-atom MD simulations.

The interactions between water molecules and the nanoporous membrane in the normal direction of the membrane ( $z$ -direction, Figure 1) bring

SSN	$h$	$h_{eff}$	$D$	$D_{eff}$	$G_0$
			1.0	-	0.7
			1.5	1.20	4.3
SL-MoS <sub>2</sub>	0.31	0.96	2.0	1.64	8.1
			2.5	2.14	12.5
			3.0	2.72	17.9
BL-MoS <sub>2</sub>	0.94	1.44	2.0	1.64	6.0
TL-MoS <sub>2</sub>	1.56	2.16	2.0	1.64	5.3
graphene	-	0.74	2.0	1.72	9.0

**Table 1:** Solid-state nanopores studied in the present work using NEMD simulations. Diameters  $D$  and  $D_{eff}$  as well as thicknesses  $h$  and  $h_{eff}$  are given in nm. Conductances  $G_0$  are given in nS.

information into the modification of the bulk water properties due to the presence of the membrane. As explained in section 2, we computed the probability distribution  $P(z)$  to find a water molecule at a certain normal distance  $z$  from the membrane. Figure 3a shows the results extracted from simulations for a graphene and a MoS<sub>2</sub> nanopore of diameter  $D = 2.0$  nm. From this distribution, we extracted the *effective* thickness of the nanoporous membrane, which represents the minimum thickness from which the water structure is significantly modified. Our definition is the following: starting from the surface of the membrane,  $P(z) \sim 0$ , the first value of  $z$  giving the bulk value of  $P$  is considered as  $h_{eff}/2$  (Figure 3a). According to our simulations, the *effective* thickness is found to be  $\sim 0.74$  nm for graphene and  $0.96$  nm for MoS<sub>2</sub> (Table 1). We performed the same analysis for bilayers and trilayers MoS<sub>2</sub> and the *effective* thicknesses are  $1.44$  and  $2.16$  nm, respectively (Table 1). It corresponds to a factor of  $\sim 3$  between  $h$  and  $h_{eff}$  for SL-MoS<sub>2</sub> whereas it is associated with a factor  $\sim 1.5$  for BL and TL-MoS<sub>2</sub>. In contrast, the diameter  $D$  has no influence on the structural properties of water in the normal direction of the membrane (data not shown) since the surface of the pore ( $S = \pi R^2 < 10$  nm<sup>2</sup>) represents a small fraction of the total surface of the nanoporous membrane ( $L_x \times L_y = 100$  nm<sup>2</sup>).

We performed the same type of analysis in order to extract the *effective* diameter of a SSN from the water in-plane radial distribution inside the pore. Figure 3b shows the results extracted from MD simulations for a graphene and a MoS<sub>2</sub> nanopore of diameter  $D = 2.0$  nm. Our definition of the *effective* diameter is the following: starting from the center of the pore which corresponds to the value  $C(\rho)_0$ , the last value of  $\rho$  for which the radial distribution completely decreases approaching the edges is considered as  $R_{eff} = D_{eff}/2$  (Figure 3b). It leads to *effective* diameters  $D_{eff}$  values of  $1.72$  and  $1.64$  nm for graphene and MoS<sub>2</sub>, respectively. Despite this difference of  $0.8$  Å for the *effective* diameter between graphene and MoS<sub>2</sub>, the profiles of water concentration are similar in shape with a maximum at  $0.80$  and  $0.75$  nm, respectively (Figure 3). The maximum is located at a larger  $\rho$  for graphene due to the significant hydrophobicity of the carbon material. Moreover, the concentration of water at the mouth of the graphene nanopore is larger than the one at the mouth of the MoS<sub>2</sub> nanopore ( $D = 2.0$  nm). These two properties can be explained by a steric effect due to the fact that Mo atoms are characterized by a larger vdW diameter than C atoms. LJ parameters  $\sigma$  of Mo and C atoms are  $3.4$  and  $4.2$  Å, respectively. It

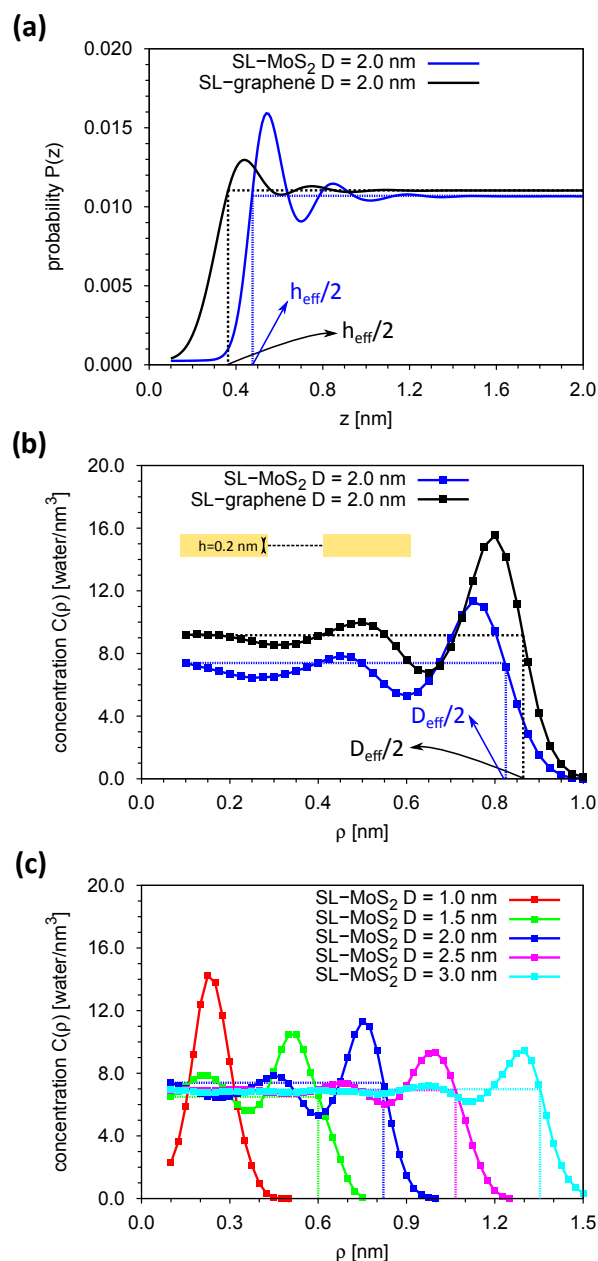


**Figure 3:** (a) Probability distribution functions  $P(z)$  of water molecules in the normal direction ( $z$ -direction) of the nanoporous membrane. Graphene is shown in black and SL-MoS<sub>2</sub> in blue for a diameter  $D = 2.0$  nm. (b) In-plane radial distribution  $C(\rho)$  of water molecules inside the nanopore. Graphene is shown in black and SL-MoS<sub>2</sub> in blue for a diameter  $D = 2.0$  nm. The inset in panel b corresponds to a schematic representation of the in-plane calculation. (c) In-plane radial distribution  $C(\rho)$  of water molecules inside single-layer MoS<sub>2</sub> nanopores of diameters  $D = 1.0$  (red),  $1.5$  (green),  $2.0$  (blue),  $2.5$  (magenta) and  $3.0$  nm (cyan). Dashed lines represent the value of the *effective* thicknesses (panel a) and diameters (panels b and c) extracted from the distributions.

corresponds exactly to the difference of *effective* diameters between the two nanopores.

For SSN made of a SL-MoS<sub>2</sub> and of different

diameters  $D$  as shown in Figure 3c, the shape of the concentration profiles is identical. The property which is modified by the increase or decrease of the diameter  $D$  of the nanopore is the length of the plateau  $C(\rho)$ , leading to larger *effective* diameters  $D_{eff}$  for larger diameters  $D$  (Table 1). For SL-MoS<sub>2</sub>, the ratio  $D_{eff}/D$  is found to be around 0.8 from MD simulations. For SSN of diameters  $D = 2.0$  nm and of different thicknesses  $h$ , *effective* diameters extracted from the water in-plane radial distribution are the same as for SL-MoS<sub>2</sub> (data not shown).

### 3.3 Concentration of ions in MoS<sub>2</sub> nanopores

Using the *effective* thickness  $h_{eff}$  of graphene and MoS<sub>2</sub> membranes, we computed the radial ionic concentration in cylindrical pores (Figure 4), as explained in section 2. The advantage of this analysis is to quantify the effect of the dangling atoms on the edges of the pore onto the concentration of ions in MoS<sub>2</sub> nanopores. As shown in Figure 4b, the radial concentration of ions inside a MoS<sub>2</sub> nanopore of diameter  $D = 2.0$  nm is characterized by a plateau starting at  $\rho = 0$  up to  $\rho_{max}$ , followed by a linear decrease from  $\rho_{max}$  to  $R_{eff}$ , the *effective* radius of the nanopore (see section 3.2). The same behavior is observed for graphene with the same diameter, except that first, the length of the plateau ( $\rho_{max}$ ) is larger than the one observed for MoS<sub>2</sub>. Second, the concentration at the center of the pore is larger for MoS<sub>2</sub> than for graphene since the volume of the cylindrical pore is larger ( $V_{cyl} = 3.0$  and  $2.3$  nm<sup>3</sup>, respectively). Third, the decrease of the concentration is faster for MoS<sub>2</sub> nanopores. It comes from the fact that Mo atoms are characterized by larger vdW diameters than C atoms, which involves a larger repulsion.

The same behavior is also observed in MoS<sub>2</sub> nanopores of different diameters  $D$ , as shown in Figure 4d. In fact, the length of the plateau is larger as the diameter increases. In addition, the concentration of ions at the center of the pore decreases with the diameter from 1.5 nm to 3 nm. For larger diameters, KCl ions tend to occupy the entire space of the pore whereas for smaller diameter they are confined at the center of the pore due to the repulsion forces involved by the edges of the pore. Finally, as already stated previously, the behavior of MoS<sub>2</sub> nanopores with a diameter  $D = 1.0$  nm is completely different. In this case, the concentration of ions is so low that it can be considered as a null concentration. For MoS<sub>2</sub> nanopores made of multiple layers, the ionic concentration profiles are similar to those of the single layer. The concentration at the

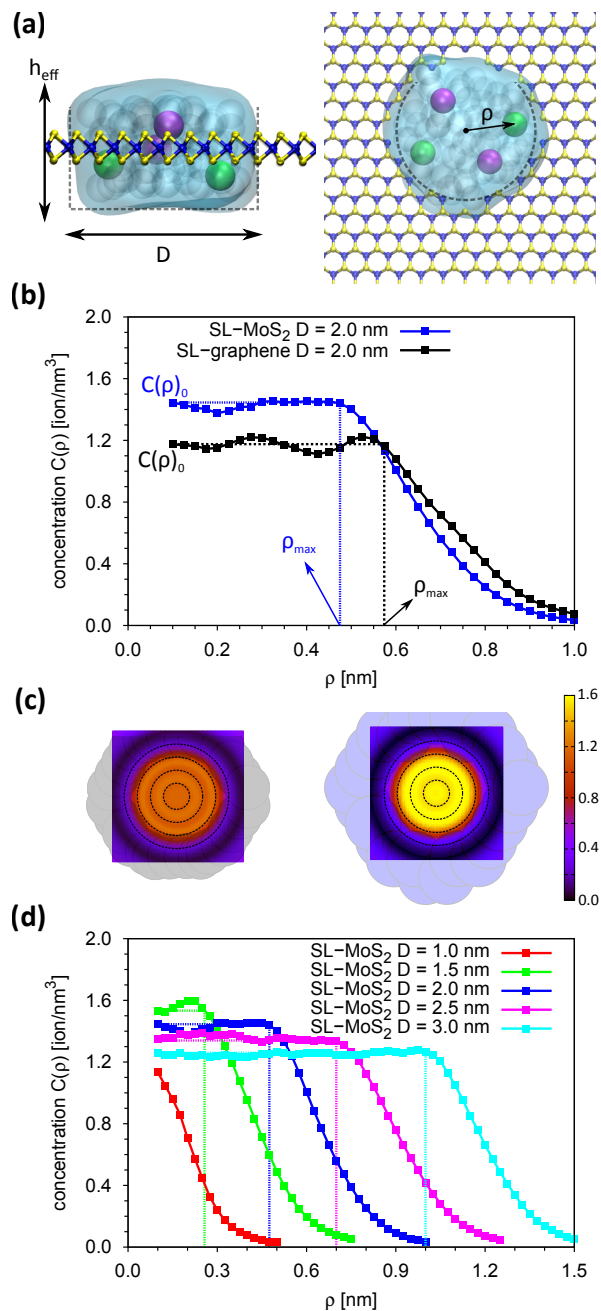


**Figure 4:** (a) Snapshot of MD simulations representing water molecules and KCl ions inside a SL-MoS<sub>2</sub> nanopore of diameter  $D = 2.0$  nm. Water molecules are represented with blue transparent spheres and a blue surface. K<sup>+</sup> and Cl<sup>-</sup> ions are represented by magenta and green spheres, respectively. (b) Radial concentration of KCl ions inside a graphene (black) and a SL-MoS<sub>2</sub> (blue) nanopore of diameter  $D = 2.0$  nm. (c) Color map of ionic concentration (colorbox in ion/nm<sup>3</sup>) in a graphene (left panel) and MoS<sub>2</sub> nanopore of diameter  $D = 2.0$  nm. Transparent black and blue circles represent spheres centered on the C and Mo atoms with a radius equal to the parameters  $\sigma_C$  and  $\sigma_{Mo}$  atoms of the LJ potential, respectively. (d) Radial concentration of KCl ions inside a SL-MoS<sub>2</sub> (blue) nanopore of diameters  $D = 1.0$  nm (red),  $1.5$  nm (green),  $2.0$  nm (blue),  $2.5$  nm (magenta) and  $3.0$  nm (cyan). Dashed lines indicate the length of the plateau  $\rho_{max}$ .

center of the pore is larger than in single-layer nanopores ( $C(\rho)_0 \sim 2.0$  ions/nm<sup>3</sup>) due to the fact that the *effective* volume of the cylinders is larger.

The main question that arises here is: what is the impact of such ionic concentration profiles on conductance drop measurements during an experiment? The answer to this question is not simple and we will provide a number of hypotheses. Consider a SL-MoS<sub>2</sub> nanopore of diameter  $D = 3.0$  nm. From the concentration profile shown in Figure 4d, we estimate the length of the plateau  $C(\rho)_0$  to be around 2.0 nm. This means that if a molecule such as a rigid double-strand B-DNA molecule ( $D_{DNA} = 2.0$  nm) translocates into the nanopore, the ionic concentration between the molecule and the edges of the pore would be  $\sim 0$ . Therefore, the conductance drop  $\Delta G$  would be similar to  $G_0$ , the open pore conductance. Compared to graphene for which the plateau is larger, the conductance drop  $\Delta G$  would be smaller than  $G_0$  despite the fact that the same object is translocated in a pore of the same diameter.

### 3.4 Comparison of MD data for MoS<sub>2</sub> nanopores with analytical model of conductance

The values of the open pore conductance  $G_0$  obtained for MoS<sub>2</sub> nanopores from NEMD simulations have been compared to the analytical model of conductance (Eq. 1) by inserting the bulk conductivity  $\sigma$  of 1M KCl. The bulk conductivity was computed by performing NEMD simulations of the ionic solution without nanopore in a simulation box of the same size as that used for the MD simulations including the nanopore. The value extracted from MD is  $\sigma = 12.8$  S m<sup>-1</sup> which is relatively close to values reported in the literature, *i.e.*  $\sigma \sim 10$ -12 S m<sup>-1</sup> [4]. The fit of the MD data was performed in two steps: first, we fitted the MD data of SL-MoS<sub>2</sub> for different diameters  $D$  using different definitions for the thickness  $h$  as shown in Figure 5a. Second, we fitted the MD data of MoS<sub>2</sub> nanopores of diameter  $D = 2.0$  nm for different thicknesses  $h$  using different definitions for the diameter  $D$  as shown in Figure 5b.

As shown in Figure 5 using the actual geometrical parameters  $h$  and  $D$  from the atomic structure, values of open pore conductance  $G_0$  are largely overestimated by the model. Moreover, using the *effective* geometrical parameters  $h_{eff}$  and  $D_{eff}$  estimated from the water distributions (see section 3.2), open pore conductances  $G_0$  are also overestimated by the model. Particularly using the

*effective* thickness  $h_{eff} = 0.96$  nm. Therefore, we decided to extract the values of  $h$  and  $D$  by fitting the model defined in Eq. 1 using  $h$  as a free parameter from  $G_0 = f(D)$  (panel a of Figure 5) and using  $D$  as a free parameter from  $G_0 = f(h)$  (panel b of Figure 5). Doing this, we got  $h_{fit} = 3.1$  nm and  $D_{fit} = 0.98$  nm, respectively. The value of  $h_{fit}$  is 10 times larger than the actual thickness of SL-MoS<sub>2</sub>, *i.e.*  $h = 0.31$  nm, whereas the value of  $D_{fit}$  is 2 times smaller than the actual diameter, *i.e.*  $D = 2.0$  nm. It means that there is a discrepancy between bulk conductivity  $\sigma$  and the pore conductivity for diameters comprised ranging from 1.5 to 3.0 nm.

As suggested by Suk and Aluru in their paper about sub-5 nm graphene nanopores [35], the bulk conductivity  $\sigma$  should be replaced in the model defined in Eq. 1 for diameters  $D \sim 2.0$  nm by an

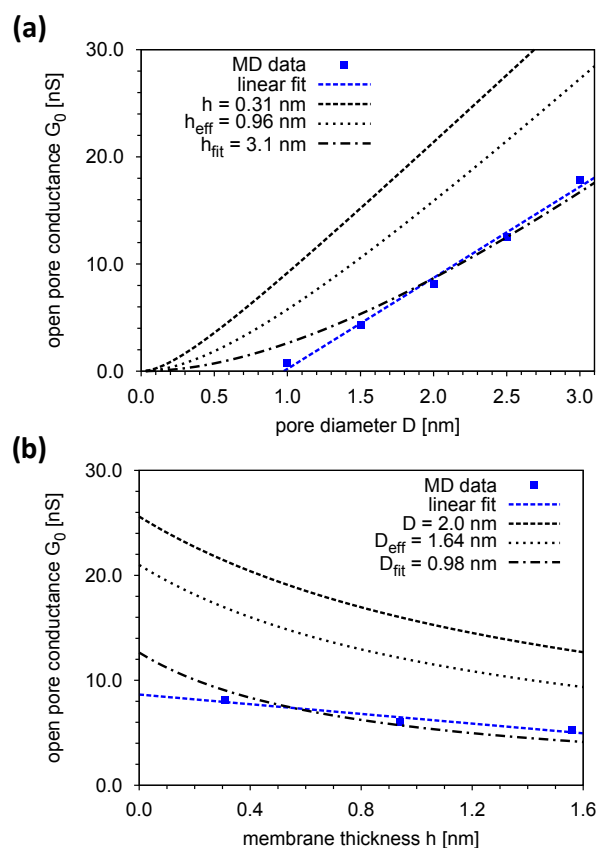


**Figure 5:** (a) Open pore conductances  $G_0$  as a function of the pore diameter  $D$  for SL-MoS<sub>2</sub> nanopores. (b) Open pore conductances  $G_0$  as a function of the membrane thickness  $h$  for MoS<sub>2</sub> nanopores of diameter  $D = 2.0$  nm. MD data are represented by blue squares. Black lines represent the results of the fit obtained using the analytical model defined in Eq. 1 using: the actual geometrical parameters (dashed line), the *effective* geometrical parameters (dotted line), the fitted geometrical parameters (dash-dotted line). Blue dashed lines represent a linear fitting of the MD data.

ionic conductivity which depends on the diameter of the pore  $\sigma(D)$ . In fact, it also depends on the thickness  $h$  for multiple layers SSN and on the interactions between the ionic solution and the 2-D materials. In the present work, the goal was not to give the exact analytical expression of  $\sigma(D, h, \dots)$  but to provide a benchmark of  $G_0$  values for further experiments. As shown in Figure 5, a linear model of conductance could also be used to represent the MD data, *i.e.*  $G_0(D) = \alpha D + \beta$  (panel a) and  $G_0(h) = \gamma h + \delta$  (panel b). It actually provides a better fit than the model defined in Eq. 1. The values of the linear fit are:  $\alpha = 8.5 \text{ nS m}^{-1}$ ,  $\beta = -8.3 \text{ nS}$ ,  $\gamma = -2.3 \text{ nS m}^{-1}$  and  $\delta = 8.6 \text{ nS}$ . Finally, from MD simulations data shown in Figure 5a, *i.e.*  $G_0 = f(D)$ , the value of the critical diameter for MoS<sub>2</sub> nanopores observed earlier in the paper (Figure 3c) can be extracted from  $G_0(D_{min}) = 0$ , leading to  $D_{min} = -\beta/\alpha = 0.98 \text{ nm}$ .

## 4 Conclusion

We have studied the ionic conductance through MoS<sub>2</sub> nanopores of different diameters ( $D = 1.0, 1.5, 2.0, 2.5$  and  $3.0 \text{ nm}$ ) and different thicknesses (single, bi- and trilayers). Using MD simulations, we extracted values of open pore conductance  $G_0$  that can be related directly to conductance drops  $\Delta G$  measured in single molecule detection experiments. If the size of the molecule to be translocated through the nanopore is similar to the diameter of the pore, we find that  $\Delta G \sim G_0$ . Therefore, there is a strong interest to provide benchmarks of conductance signals using MD simulations. Here, we provide linear conductance models to estimate  $G_0 = f(D)$  and  $G_0 = f(h)$  and we show that there exists a critical diameter  $D_{min} = 1.0 \text{ nm}$  for SL-MoS<sub>2</sub> nanopores. In addition, these models extracted from the present MD simulations allow us to estimate the geometrical parameters of MoS<sub>2</sub> nanopores from conductance measurements. The estimation of the pore diameter and thickness of the nanoporous membranes from conductance measurements is commonly used in experiments with the analytical model presented in Eq. 1. This approach can lead to large error bars according to the present computational study.

**Acknowledgements:** The calculations were performed using HPC resources from DSI-CCuB (Université de Bourgogne). This work was supported by a grant from the Air Force Office of Scientific Research (AFOSR), as part of a joint program with the Directorate for Engineering of the National

Science Foundation (NSF), Emerging Frontiers and Multidisciplinary Office grant No. FA9550-17-1-0047. The authors also thank the Conseil Régional de Bourgogne for the funding (grant PARI Nano2bio).

### References:

- [1] C. Dekker, Solid-state nanopores, *Nat. Nanotechnol.* 2, 2007, pp. 209–215.
- [2] H. Arjmandi-Tash, L. Belyaeva and G. Schneider, Single molecule detection with graphene and other two-dimensional materials: nanopores and beyond, *Chem. Soc. Rev.* 45, 2016, pp. 476–493.
- [3] J. K. Rosenstein, M. Wanunu, C. A. Merchant, M. Drndić, K. L. Shepard, Integrated nanopore sensing platform with sub-microsecond temporal resolution, *Nat. Methods* 9, 2012, pp. 487–492.
- [4] J. Rodríguez-Manzo, M. Puster, A. Nicolai, V. Meunier, M. Drndić, DNA translocation in nanometer thick silicon nanopores, *ACS. Nano* 9, 2015, pp. 6555–6564.
- [5] S. W. Kowalczyk, A. Y. Grosberg, Y. Rabin and C. Dekker. Modeling the conductance and DNA blockade of solid-state nanopores, *Nanotechnology* 22, 2011, pp. 315101.
- [6] M. Wanunu, T. Dadosh, V. Ray, J. Jin, L. McReynolds, M. Drndić, Rapid electronic detection of probe-specific microRNAs using thin nanopore sensors, *Nat. Nanotechnol.*, 5, 2010, pp. 807–814.
- [7] K. Venta, G. Shemer, M. Puster, J. A. Rodríguez-Manzo, A. Balan, J. K. Rosenstein, K. Shepard, M. Drndić, Differentiation of short, single-stranded DNA homopolymers in solid-state nanopores, *ACS Nano*, 7, 2013, pp. 4629–4636.
- [8] E. A. Manrao, I. M. Derrington, A. H. Laszlo, K. W. Langford, M. K. Hopper, N. Gillgren, M. Pavlenok, M. Niederweis, J. H. Gundlach, Reading DNA at single-nucleotide resolution with a mutant MspA nanopore and phi29 DNA polymerase, *Nat. Biotechnol.* 30, 2012, pp. 349–353.
- [9] C. A. Merchant, K. Healy, M. Wanunu, R. Vishva, N. Peterman, J. Bartel, M. D. Fischbein, K. Venta, Z. Luo, A. T. C. Johnson, M. Drndić, DNA translocation through graphene nanopores, *Nano Lett.* 10, 2010, pp. 2915–2921.

- [10] G. F. Schneider, S. W. Kowalczyk, V. E. Calado, G. Pandraud, H. W. Zandbergen, L. M. K. Vandersypen, C. Dekker, DNA translocation through graphene nanopores, *Nano Lett.* 10, 2010, pp. 3163-3167.
- [11] S. Garaj, W. Hubbard, A. Reina, J. Kong, D. Branton, J. A. Golovchenko, Graphene as a sub-nanometer trans-electrode membrane, *Nature* 467, 2010, pp. 190-193.
- [12] S. J. Heerema, G. F. Schneider, M. Rozemuller, L. Vicarelli, H. W. Zandbergen, C. Dekker, 1/f noise in graphene nanopores, *Nanotechnology* 26, 2015, pp. 074001.
- [13] A. Aksimentiev, Deciphering ionic current signatures of DNA transport through a nanopore, *Nanoscale* 2, 2010, pp. 468-483.
- [14] C. Sathe, X. Zou, J.-P. Leburton, K. Schulten, Computational investigation of DNA detection using graphene nanopores, *ACS Nano* 5, 2011, pp. 8842-8851.
- [15] D. B. Wells, M. Belkin, J. Comer, A. Aksimentiev, Assessing graphene nanopores for sequencing DNA, *Nano Lett.* 12, 2012, pp. 4117-4123.
- [16] W. Lv, S. Liu, X. Li, R. Wu, Spatial blockage of ionic current for electrophoretic translocation of DNA through a graphene nanopore, *Electrophoresis* 35, 2014, pp. 1144-1151.
- [17] R. Lv, J. A. Robinson, R. E. Schaak, D. Sun, Y. Sun, T. E. Mallouk, M. Terrones, Transition Metal Dichalcogenides and Beyond: Synthesis, Properties, and Applications of Single- and Few-Layer Nanosheets, *Acc. Chem. Res.* 48, 2015, pp. 56-64.
- [18] K. Liu, J. Feng, A. Kis, A. Radenovic, Atomically thin molybdenum disulfide nanopores with high sensitivity for DNA translocation, *ACS Nano* 8, 2014, pp. 2504-2511.
- [19] A. B. Farimani, K. Min, N. R. Aluru, DNA base detection using a single-layer MoS<sub>2</sub>, *ACS Nano* 8, 2014, pp. 7914-7922.
- [20] J. W. Jiang, Parametrization of Stillinger-Weber potential based on valence force field model: application to single-layer MoS<sub>2</sub> and black phosphorus, *Nanotechnology* 26, 2015, pp. 315706.
- [21] W. L. Jorgensen, J. Chandrasekhar, J. Madura, R. W. Impey, M. L. Klein, Comparison of simple potential functions for simulating liquid water, *J. Chem. Phys.* 79, 1983, pp. 926-935.
- [22] I. S. Joung, T. E. Cheatham, Determination of alkali and halide monovalent ion parameters for use in explicitly solvated biomolecular simulations, *J. Phys. Chem. B* 112, 2008, pp. 9020-9041.
- [23] T. Liang, S. R. Phillpot, S. B. Sinnott, Parametrization of a reactive many-body potential for Mo-S systems, *Phys. Rev. B* 79, 2009, pp. 245110.
- [24] M. Heiranian, A. B. Farimani, N. R. Aluru, Water desalination with a single-layer MoS<sub>2</sub> nanopore, *Nat. Commun.* 6:8616, 2015.
- [25] J. Tersoff, New empirical approach for the structure and energy of covalent systems, *Phys. Rev. B* 37, 1988, pp. 6991-7000.
- [26] R. Saito, R. Matsuo, T. Kimura, G. Dresselhaus, M. S. Dresselhaus, Anomalous potential barrier of double-wall carbon nanotube, *Chem. Phys. Lett.* 348, 2001, pp. 187-193.
- [27] S. Plimpton, Fast parallel algorithms for short-range molecular dynamics, *J. Comp. Phys.* 117, 1995, pp. 1-19.
- [28] W. C. Swope, H. C. Andersen, P. H. Berens, K. R. Wilson, A computer simulation method for the calculation of equilibrium constants for the formation of physical clusters of molecules: Application to small water clusters, *J. Chem. Phys.* 76, 1982, pp. 637-649.
- [29] S. Nosé, A unified formulation of the constant temperature molecular-dynamics methods, *J. Chem. Phys.* 81, 1984, pp. 511-519.
- [30] W. G. Hoover, Canonical dynamics: Equilibrium phase-space distributions, *Phys. Rev. A* 31, 1985, pp. 1695-1697.
- [31] R. W. Hockney, J. W. Eastwood, *Computer Simulation Using Particles*, Adam-Hilger, New York 1989.
- [32] J.-P. Ryckaert, G. Ciccotti, H. J. C. Berendsen, Numerical integration of the cartesian equations of motion of a system with constraints: molecular dynamics of n-alkanes, *J. Comp. Phys.* 23, 1977, pp. 327-341.
- [33] E. R. Cruz-Chu, A. Aksimentiev, K. Schulten, Ionic current rectification through silica nanopores, *J. Phys. Chem. C* 113, 2009, pp. 1850-1862.
- [34] T. Sumikama, Origin of the shape of current-voltage curve through nanopores: a molecular dynamics study, *Sci. Rep.* 6, 2016, pp. 25750.
- [35] M. E. Suk, N. R. Aluru, Ion transport in sub-5-nm graphene nanopores, *J. Chem. Phys.* 140, 2014, pp. 084707.